

## CHAPTER 13: ABSOLUTE CHRONOLOGY

*by Alex Bayliss and Gill Hey*

The principal aim of the scientific dating programme was to identify which parts of the environmental sequences from the floodplain could be related to the Roman and Iron Age archaeology reported elsewhere in this volume. Rather more Iron Age activity was identified than initially envisaged. For example, the middle Iron Age cemetery was originally thought to be Anglo-Saxon in date (Hey *et al* 1999), and the stone causeway on site 9 was thought to be Bronze Age on the basis of the associated finds (Hey and Bell 1999).

### **Radiocarbon Dating** *by Alex Bayliss, Chris Bronk Ramsey, Gordon Cook, and Gerry McCormac*

Forty-four radiocarbon determinations have been obtained on samples of Iron Age and Roman date from Yarnnton.

#### *Sample preparation and measurement*

Sixteen samples were processed by the Radiocarbon Dating Laboratory of the Queen's University, Belfast between 1994 and 2001, according to methods outlined in Longin (1971), Pearson (1984), and McCormac (1992), and measured using Liquid Scintillation Counting (Noakes *et al* 1965). Nine samples were processed by the Scottish Universities Research and Reactor Centre at East Kilbride between 1998 and 2002. These were prepared using the methods outlined in Stenhouse and Baxter (1983) and also measured using liquid scintillation spectrometry (Noakes *et al* 1965). Nineteen samples were dated by the Oxford Radiocarbon Accelerator Unit between 1992 and 2001. These were prepared and measured using methods outlined in Hedges *et al* (1989) and Bronk Ramsey and Hedges (1997). The pre-treatment method used for bone samples was a collagen extraction (Law and Hedges 1989; Hedges *et al* 1989) followed by gelatinisation and separation by filtration (Bronk Ramsey *et al* 2000).

#### *Quality Assurance*

All three laboratories maintain continual programmes of quality assurance procedures, in addition to participation in international inter-comparisons (Rozanski *et al* 1992; Scott *et al* 1998). These tests indicate no laboratory offsets and demonstrate the validity of the precision quoted.

#### *Results*

The results are given in Table 13.1, and are quoted in accordance with the international standard known as the Trondheim convention (Stuiver and Kra 1986). They are conventional radiocarbon ages (Stuiver and Polach 1977).

#### *Calibration*

The calibrations of these results, relating the radiocarbon measurements directly to calendar dates, are given in Table 13.1 and in outline in Figures 13.1–13.7. All have been calculated using the calibration curve of Stuiver *et al* (1998) and the computer program OxCal (v3.5) (Bronk Ramsey 1995; 1998; 2001). The calibrated date ranges cited in the text are those for 95% confidence. They are quoted in the form recommended by Mook (1986), with the end points rounded outwards to 10 years. The ranges quoted in italics are *estimated date ranges* derived from mathematical modelling of archaeological problems (see below). The ranges in Table 13.1

have been calculated according to the maximum intercept method (Stuiver and Reimer 1986), all other ranges are derived from the probability method (Stuiver and Reimer 1993).

### **Optically Stimulated Luminescence (OSL) Analysis by Julie Rees-Jones**

Nine OSL samples were taken from palaeochannel deposits on Yarnton floodplain and analysed as part of a doctoral thesis at the Oxford University Research Laboratory (Rees-Jones 1995). These results have been integrated with those of other scientific dating methods.

Optical dating can be used to determine the time elapsed since a buried sedimentary context was last exposed to light by using measurements of the optically stimulated luminescence signal from crystals in the sediments to calculate the radiation dose received since zeroing (Huntley *et al* 1985). Optically stimulated luminescence (OSL) is the light given out by crystals on exposure to a standard light source, due to the release of stored energy resulting from prior exposure to ionising radiation (alpha and beta particles of gamma rays). The intensity of the OSL signal is proportional to the radiation dose that the crystals have received since the stored energy was last set to zero by exposure to daylight.

This can be used to date a sediment as they contain crystals of quartz and feldspar which have a luminescence signal that will be zeroed when exposed to sunlight, thus at deposition of the sediment the luminescence signal is set to zero. The sediment then becomes buried and is kept dark. During burial the sediment is exposed to naturally occurring radiation and the luminescence signal grows, which can be measured in the laboratory.

#### *Measurement procedures*

The samples were collected so as to minimise light exposure, by driving a steel core into a section face. The ends of the sediment cores that were exposed to light at collection were discarded in the laboratory, where sample preparation took place under restricted lighting conditions. The samples were treated with dilute hydrochloric acid and hydrogen peroxide, rinsed in distilled water and methanol and the 4–11µm grains separated by their settling time in acetone.

The luminescence signal from the samples was measured by exposure to infrared light (IRSL) using an Elsec optical dating system (Spooner *et al* 1990), with aliquots normalised by the counts produced from a short infrared shine applied to the natural signal.

The first stage was to estimate the preheat time at 160°C appropriate for dating each sample. Preheating is required, as laboratory irradiation fills unstable traps not present in the natural signal due to fading over the burial period. Determining the appropriate preheat involved irradiating aliquots with various beta doses ( $^{90}\text{Sr}$ – $^{90}\text{Y}$  source) and making short shine measurements (0.2s) after preheats of increasing duration. For each preheat time an additive growth curve was constructed and an equivalent dose (the beta dose giving rise to a luminescence signal equivalent to that of the natural signal) calculated. These equivalent doses or EDs increase in value with preheat time until the time is sufficient to remove all charge unstable over burial time. The results showed that a preheat of 4 h at 160°C was required for most samples, with sample 957b requiring only 2 h and 957e requiring 6 h.

Further aliquots were then used to construct an additive beta growth curve and a similar additive alpha growth curve (using an  $^{241}\text{Am}$  foil source), the previous determined preheat at 160°C being

used. The beta and alpha EDs were determined by a linear fit to the growth curves. The alpha ED was used to calculate alpha particle effectiveness at creating a luminescence signal (a-value), as alpha radiation is less effective than beta.

The preheating procedure can cause transfer of charge from unbleachable to bleachable traps, which results in additional OSL signal, which must be corrected for. This is achieved by bleaching the beta growth curve aliquots then re-dosing and preheating them to construct a second growth curve from which an intercept correction is determined (Rees-Jones and Tite 1994). This correction also allows for any residual, hard to bleach signal. The intercept correction was subtracted from the ED to give the palaeodose, the radiation dose the sample has received since last bleached.

The radioactive dose received by the samples was determined by on-site gamma spectrometry, as problems were experienced in calculating the water contents of the sediments due to their high clay contents.

### *Results*

The measured values for the palaeodose (P), a-value, and dose rate are shown in Table 13.2 together with the dates calculated. The errors quoted are at the 68% confidence level and include both random and systematic errors (Aitken 1985).

## **Natural Remanent Magnetisation** *by Neil Linford and Paul Linford*

### *Sampling and measurement*

Forty orientated 10cc samples were initially recovered from the section of a heavily alluviated ditch where an organic rich black layer had accumulated at the base of the feature (Site 25, ditch segment 12012, part of ditch group 12036) (see Fig. 00.00) to investigate the magnetic properties of sediments from the site (*cf* Linford 1994). Measurements on these samples confirmed that, in contrast to the overlying alluvium, the organic rich layer at the base of the ditch contained a significant concentration of magnetic minerals and also retained a stable Natural Remanent Magnetisation (NRM). In an attempt to obtain a statistically more valid archaeomagnetic date from this organic rich layer a second archaeological section through the feature was cut (Ditch group 12036) and an additional 32 samples recovered.

The NRM of each sample was measured with a Geofysika JR5A automated spinner magnetometer. Repeat measurements were then made following the progressive removal of the NRM through triple axis AF field demagnetisation using a DTech D2000 AF demagnetiser to maximum peak field of 100mT.

### *Determination of the archaeomagnetic date*

Figure 13.8 shows the progressive demagnetisation of a representative sample (BAS230) and demonstrates the presence of a single, stable magnetisation vector. A mean direction for the magnetisation of the sediment was then calculated from similar measurements made on a total of 20 samples from section 12036 that were found to retain a stable magnetisation. The mean direction is shown graphically superimposed over the archaeomagnetic calibration curve for the United Kingdom (Fig 13.8 (D)) and suggests a date of 185 cal BC to 95 cal BC at 63% confidence (215 cal BC to 85 cal BC at 95% confidence).

### *Significance of the magnetic remanence carrier*

Generally, the remanence carriers within a sediment are derived from translocated magnetic minerals from geological and soil units within the local catchment, as opposed to the formation of new magnetic material within the sediment itself. The preferential alignment of these magnetic minerals with the ambient magnetic field can certainly produce a stable NRM even under relatively turbid fluvial conditions (eg Ellis and Brown 1998).

In this case, however, additional analysis confirms the dominant NRM carriers to be a mixture of iron sulphide (most probably greigite) and bacterially derived magnetite. As the formation of both of these magnetic phases occurs only under micro-aerobic conditions, and usually in close association with organic matter, it is proposed that the resultant NRM is entirely post-depositional. Unlike archaeomagnetic dates derived from thermoremanent features the NRM recorded from the formation of *in situ* magnetic minerals may not, necessarily, be related to the construction or use of the feature in which the sediment has formed. In addition, the survival of greigite indicates that the sediment has been deoxygenated since the formation of the NRM suggesting this event was, perhaps, precipitated by a rapid change of environmental conditions, such as the onset of floodplain conditions and the sealing of the ditch cut by alluvium.

### **General approach to analysis and interpretation**

The approach to chronology adopted here is unashamedly interpretative. The simple date ranges provided by the various scientific dating methods are accurate estimates of the dates of the samples processed, but it is the dates of the archaeological events represented by those samples which are significant. Methodology is now available which allows us to combine the results of the scientific analyses with other information, such as stratigraphy, to produce realistic estimates of dates of archaeological interest. It should be emphasised that these distributions and ranges are not absolute, they are interpretative *estimates*, which can and will change as further data become available and as other researchers choose to model the existing data from different perspectives. These *estimated date ranges* (posterior density estimates), which combine the scientific and archaeological information, are given *in italics* to distinguish them from date ranges dependent on scientific information alone.

The technique used is a form of Markov Chain Monte Carlo sampling, and has been applied using the program OxCal v3.5 (<http://units.ox.ac.uk/departments/rlaha/>), which uses a mixture of the Metropolis-Hastings algorithm and the more specific Gibbs sampler (Gilks *et al* 1996; Gelfand and Smith 1990). Details of the algorithms employed by this program are available from the on-line manual or in Bronk Ramsey (1995; 1998; 2001), and fully worked examples are given in the series of papers by Buck *et al* (1991; 1992; 1994). The algorithms used in the models described below can be derived from the structure shown in Figures 13.1–13.7.

### **Analysis and interpretation**

#### *Worton Rectory Farm Cemetery*

High-precision radiocarbon measurements are available from nine articulated skeletons from across a middle Iron Age inhumation cemetery, located to the east of the Iron Age settlement (Fig 13.1A). The cemetery appears to comprise two distinct groups: a northern group of fifteen individuals (of which five were dated), and a southern group with ten bodies (of which

two were sampled; Hey *et al* 1999). In addition, ten inhumations were ‘outliers’ which were scattered along the southern and eastern edge of the settlement, and two samples were derived from this group. For the purposes of the chronological model discussed here, all these burials are treated as a single group. The introduction of MCMC sampling, in particular the Metropolis-Hastings algorithm, and improved procedures for converging models since v2.18 of OxCal (Bronk Ramsey 1998; 2001), means that we have been able to remodel this data to produce absolute estimates for the date of the cemetery.

This model suggests that burial started in 420-230 cal BC (95% probability) and ended in 290-150 cal BC (95% probability), spanning a period of 1-220 years (95% probability)(Fig 13.1B). It is most likely, however, that this cemetery was used for a relatively short period during the third century BC (Fig 13.1A).

Two Roman burials were also dated; one, a south-north extended inhumation of a decapitated woman, the other an extended north-south young female. Both of these were located to the south-east of the Roman settlement, and date to cal AD 240-385 (95% confidence; UB-3777) and cal AD 130-325 (95% confidence; UB-3921).

#### *Oxey Mead*

A palaeochannel sequence on Oxey Mead was dated (Section 3; Fig 13.2). The lowest organic deposit within the channel yielded a radiocarbon date of 200 cal BC – 10 cal AD (95% confidence; OxA-10690). Above was greenish-brown inorganic silt (layer 3/7), which dated to the later Roman or early Saxon period (OxA-7360).

#### *Floodplain Section A*

A sequence of organic silts containing structural and dumped wood was excavated adjacent to, and south of, Yarnton Floodplain, site 1. The absolute dating information relating to the Iron Age and Roman deposits in this channel is shown in Table 13.1 and Figure 13.3.

The earliest organic silts within the channel dated to the mid to late Bronze Age (layer 32). A small wooden revetment on the southern side of the channel (structure 116) is dated to 800 – 760 cal BC (UB-4062). A second post from this structure yielded a late Neolithic/early Bronze Age date, but must be reused in this context. On the south side of the channel, an area of collapsed wattle work was discovered, which is dated to the late Bronze Age/early Iron Age (structure 119). A period of ponding and silting followed, which appears to be early Iron Age on the basis of radiocarbon determinations from roundwood debris deposited in the sediments (layer 115). Further silting appears to contain redeposited wood, as GU-5850 and GU-5855 both have poor agreement with their stratigraphic positions (A=0.0% and A=0.0%; Fig 13.3; Bronk Ramsey 1995). Structure 112 was driven through these silts and has produced four statistically inconsistent radiocarbon determinations (T'=116.9; T'(5%)=7.8; df=3; Ward and Wilson 1978). UB-4677 is significantly earlier than the other three posts and is in poor agreement with its stratigraphic position (A=0.0%); it was probably reused. OxA-3644 is also slightly earlier than UB-4060 and UB-4676 (which are statistically consistent; T'=2.9; T'(5%)=3.8; df=1), and this may also be reused, although there could be an old-wood offset as the part of the oak tree dated is not known. The structure appears to be early Iron Age in date. Organic silts continued to accumulate in the channel from the middle Iron Age (OxA-10711, layer 37; OSL-866b, layer 11), becoming inorganic during the Roman period (OSL-866a, layer 10).

The quantity of redeposited Bronze Age wood must reflect activity within this channel

associated with the settlement of this date on the north bank (Site 2; Hey *et al* in prep).

#### *Floodplain Section B*

The same palaeochannel was sectioned further to the west, between Floodplain Sites 2 and 4. One of these sections was dated (Table 13.1; Fig 13.4).

Organic sediment began to accumulate in the middle Iron Age (*OxA-10691*), and continued to build up into the early Roman period (layers 8 and layer 7; *OSL-957a*, *OSL-957b*, and *OxA-4816*). Slightly organic alluvium was deposited in the later Roman and, possibly, sub-Roman periods (layer 6).

#### *Site 2 (alluviation)*

Inorganic alluvium began to accumulate in the surviving hollows over cut features on Site 2 in the middle Iron Age (*OxA-6616*; Fig 13.5). Overbank alluvium was deposited from the late Iron Age/early Roman period (*OxA-6618*).

#### *Causeways: Site 9*

A sequence of deposits located on Site 9 seem to represent crossing places of a palaeochannel, replaced and repaired over time. The chronological model for this activity is shown in Figure 13.6.

The earliest structure recorded here is represented by a row of stakes (*OxA-10629*) and associated brushwood debris (*OxA-10628*). This is dated to *400-340 cal BC (30% probability)* or *330-230 cal BC (65% probability)*. This was sealed by a substantial limestone causeway. A middle Bronze Age side-looped spearhead ([Northover, Chapter 15](#)) was recovered from beneath the stone of the causeway. Waterlogged plant remains packed within the socket of this spearhead were dated to *400-340 cal BC (30% probability)* or *330-230 cal BC (65% probability; OxA-9377)*.

Parallel uprights and horizontal handrail pieces were assembled along the length of the stone causeway, probably as part of its initial construction. Three samples were submitted from this structure (*GU-5852; GU-5853; and GU-5883*), dating it to *370-340 cal BC (10% probability)* or *320-200 cal BC (85% probability)*. A deposit of animal bone, much of which was butchered, was recovered on top of the stone causeway (*OxA-8703-4*). These samples produced sufficient collagen for dating, unlike all other bone so far submitted from the floodplain at Yarnton. This is probably because of the localised effect of the limestone of the causeway. They show that this activity took place between *360-320 cal BC (9% probability)* or *310-160 cal BC (86% probability)*.

It appears that this causeway was in use during the middle Iron Age, and was constructed in *380-210 cal BC (95% probability)*.

#### *Trench 37*

A boundary ditch was uncovered crossing the Cassington floodplain for 300m. It was recut on two occasions, and towards its southern end it approached a palaeochannel. Lower deposits within each cut were organic, containing waterlogged seeds. Inorganic silts and alluvium fill the upper parts of the ditch, which was sealed by Roman ploughsoil. The chronological model for this ditch is shown in Figure 13.7.

Two plant macrofossils were submitted for radiocarbon dating from successive fills of the

first recut of the ditch (OxA-10708 and OxA-10707). These suggest that this recut occurred in *370-110 cal BC (95% probability)*. At this time conditions in the ditch, although waterlogged, were slightly aerobic (as shown by snails of flowing water species). The formation of greigite, dated by the NRM (see Linford and Linford above), demonstrates that these deposits had become de-oxygenated by *205-105 cal BC (42% probability)* or *95-75 cal BC (53% probability)*. It seems most likely that the creation of the greigite occurred when the deposits in the ditch became compressed as a result of alluviation in this area.

It should be noted that this alluviation probably occurs slightly later than the earliest alluviation on site 2 (see above). This is to be expected as site 2 is more low lying.

Draft

Figure 13.1A. Probability distributions of dates from the Worton Rectory Farm cemetery. Each distribution represents the relative probability that an event occurred at a particular time. For each of the dates two distributions have been plotted, one in outline, which is the result produced by the scientific evidence alone, and a solid one, which is based on the chronological model used. The large square brackets down the left-hand side along with the OxCal keywords define the overall model exactly.

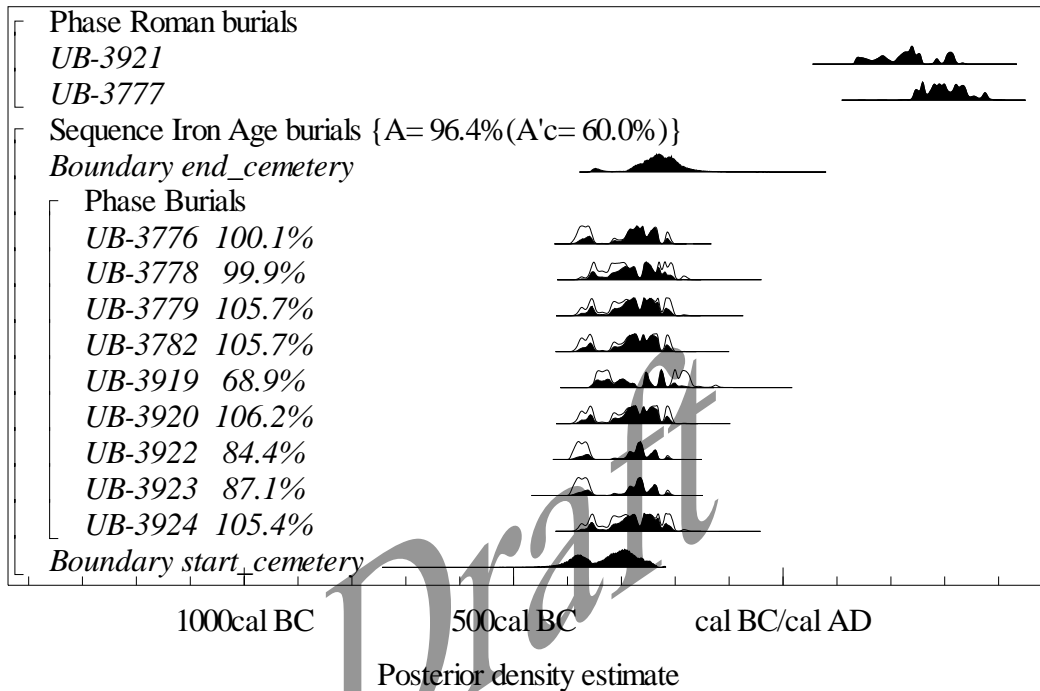
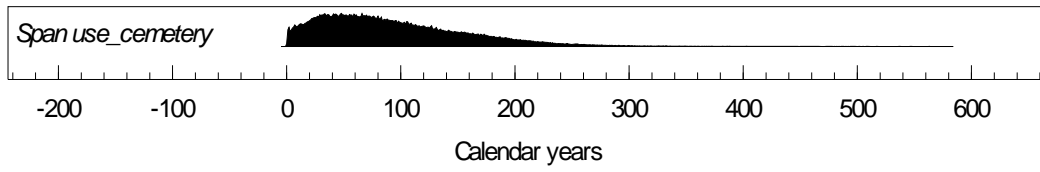
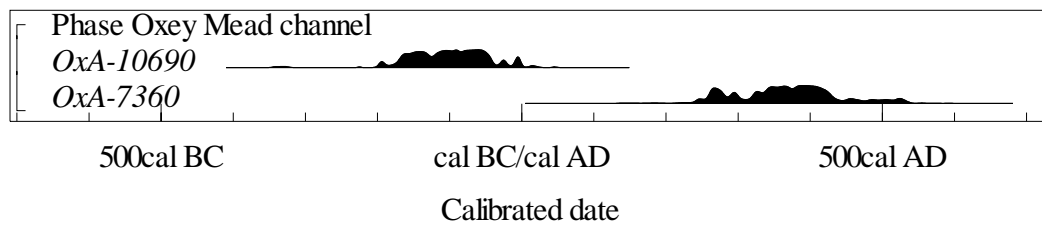


Figure 13.1B. Probability distribution of the number of years during which the cemetery was in use, derived from the model shown in Fig. 13.1A.



Draft

Figure 13.2. Probability distributions of calibrated radiocarbon dates from Oxy Mead (Stuiver and Reimer 1993).



Draft

Figure 13.3. Probability distributions of dates from Floodplain Section A. The format is identical to Fig.13.1A. Dates followed by question mark have been calibrated (Stuiver and Reimer 1993), but not included in the chronological model for reasons explained in the text. The large square brackets down the left-hand side along with the OxCal keywords define the overall model exactly.

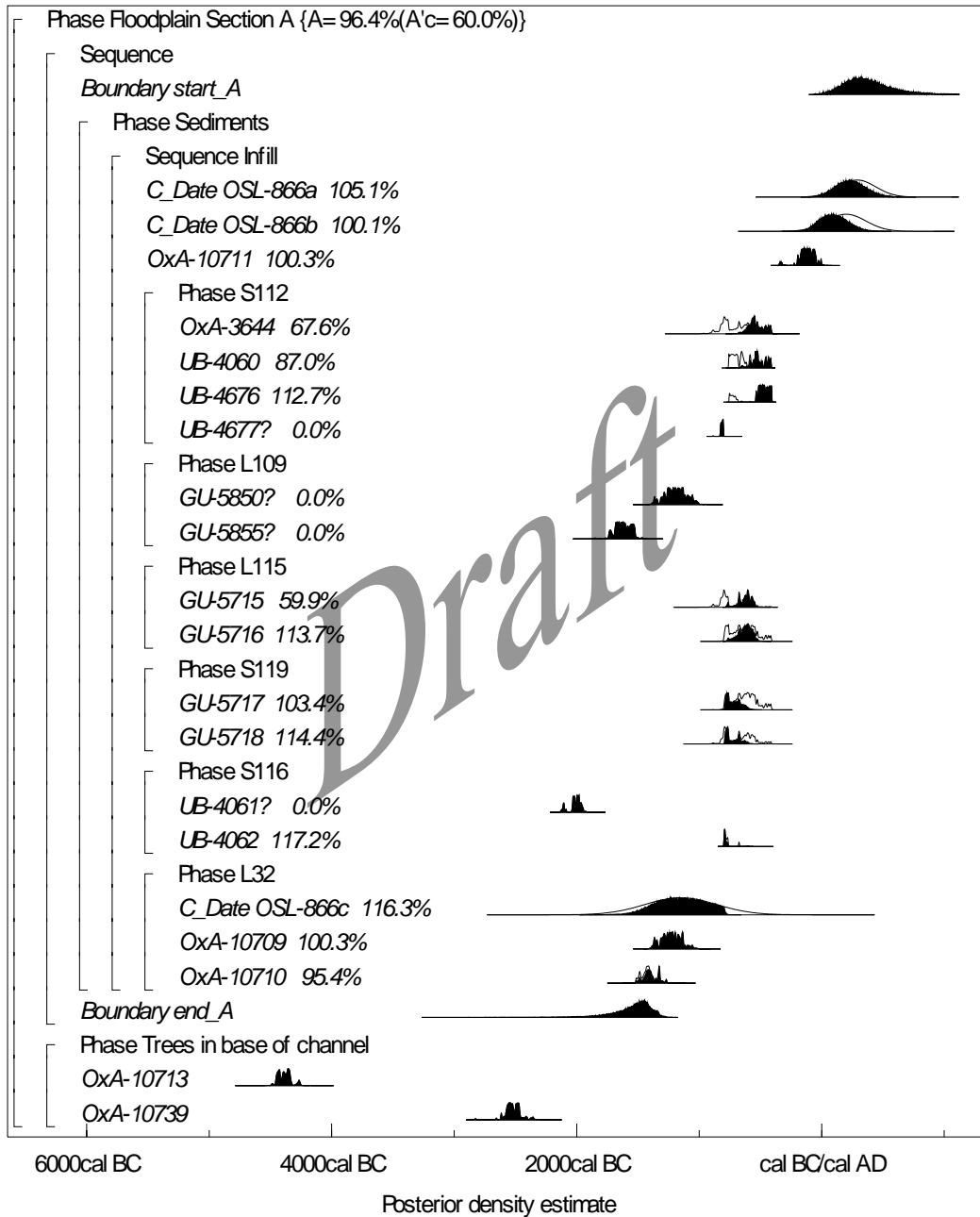
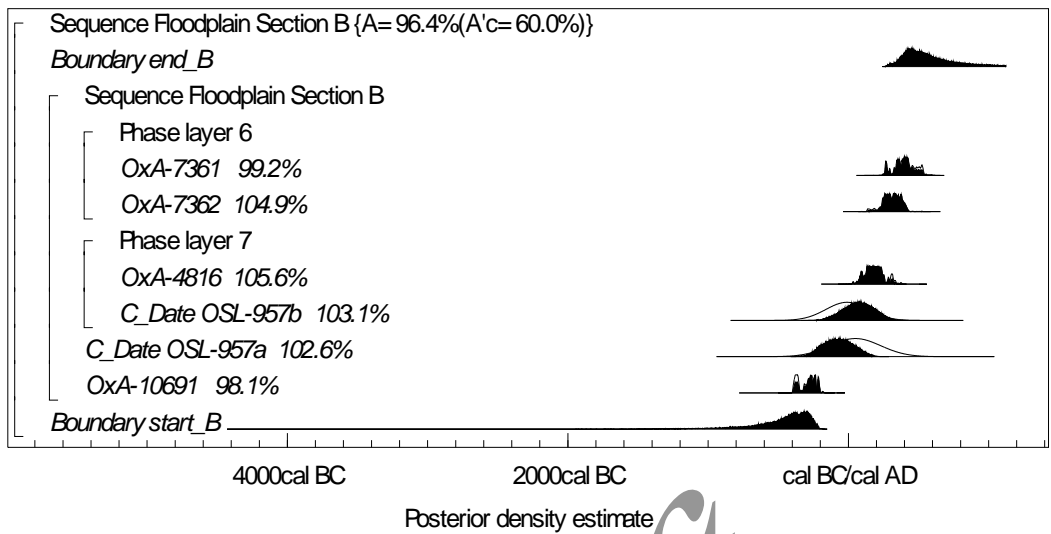
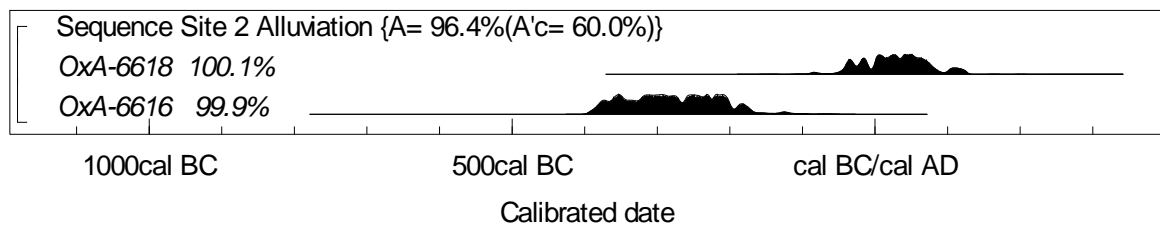


Figure 13.4. Probability distributions of dates from Floodplain Section B. The format is identical to Fig.13.1A. The large square brackets down the left-hand side along with the OxCal keywords define the overall model exactly.



Draft

Figure 13.5. Probability distributions of dates from the floodplain alluvium over Site 2. The format is identical to Fig. 13.1A. The large square brackets down the left-hand side along with the OxCal keywords define the overall model exactly.



Draft

Figure 13.6. Probability distributions of dates from the causeways on Site 9. The format is identical to Fig. 13.1A. The large square brackets down the left-hand side along with the OxCal keywords define the overall model exactly.

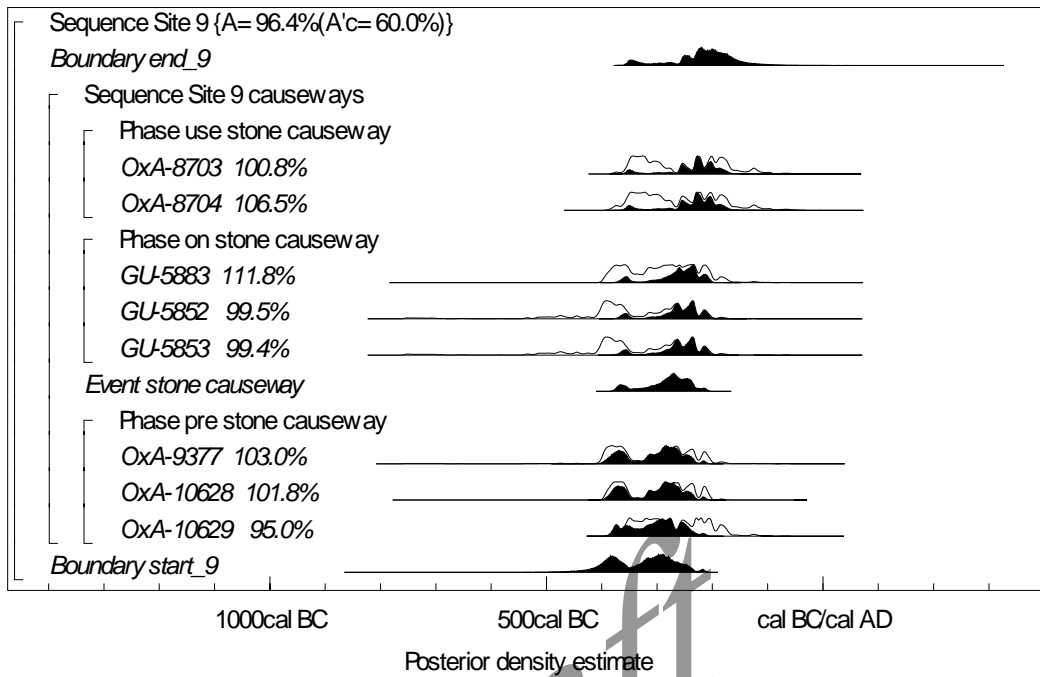
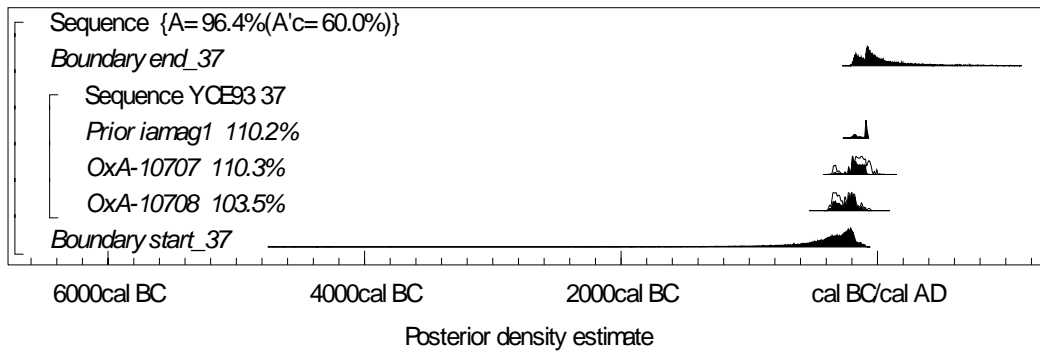


Figure 13.7. Probability distributions of dates from Trench 37. The format is identical to Fig. 13.1A. The large square brackets down the left-hand side along with the OxCal keywords define the overall model exactly.



Draft

Figure 13.8. NRM data for samples collected from the organic rich layer at the base of the alluviated ditch (section 12036). AF demagnetisation behaviour is shown for a single representative sample (BAS230) including (A) the loss of intensity and stability of remanence represented as both Zijdeveld (B) and stereonet (C) projections. The lower figure (D) shows a graphical representation of the mean calculated from all samples superimposed over the UK archaeomagnetic calibration curve. The data suggests a date of 185 cal BC to 95cal BC at 63% confidence (215 cal BC to 85 cal BC at 95% confidence).

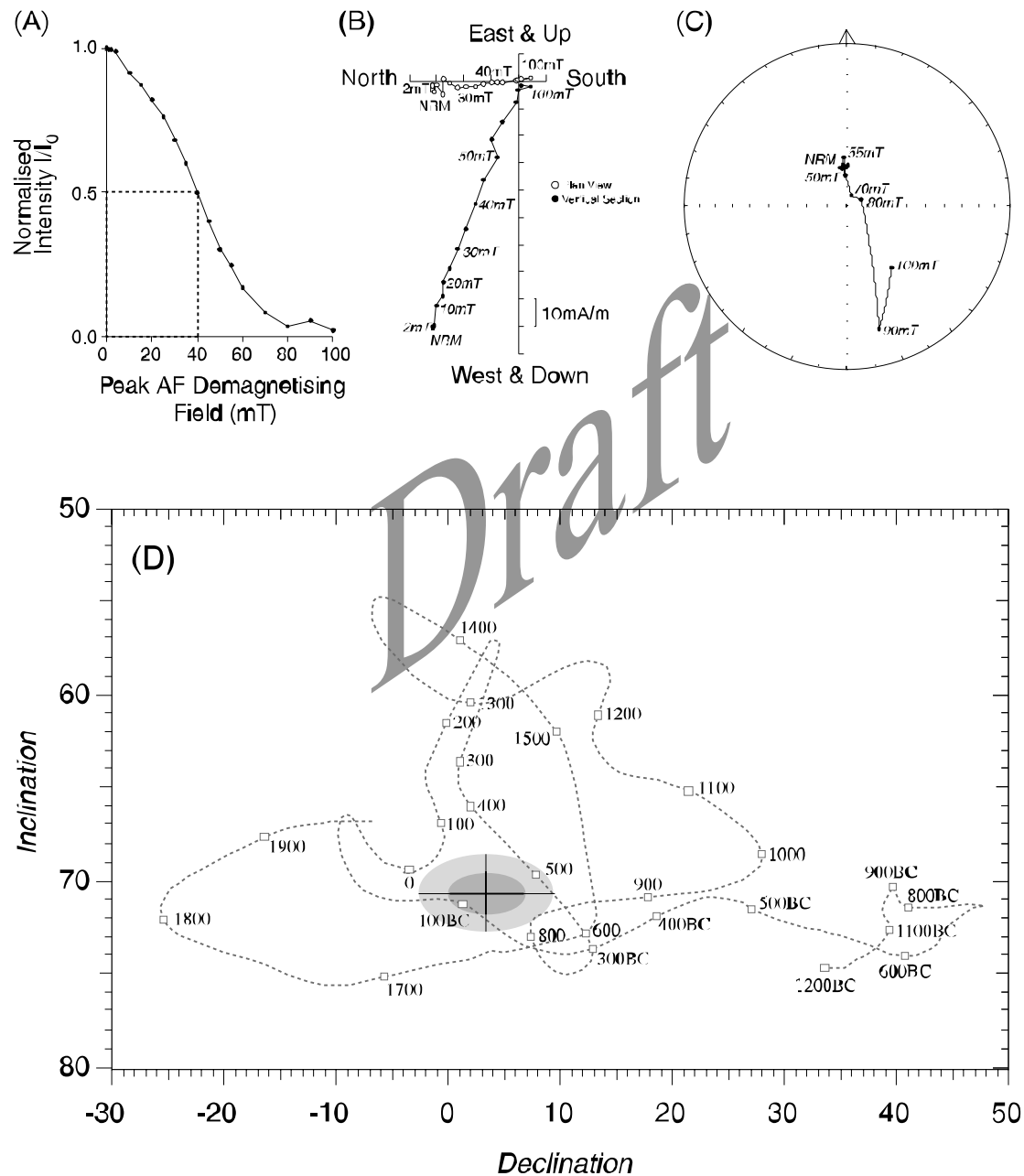


Table 13.1: Radiocarbon determinations

Site	Lab no.	Context no	Radiocarbon Age BP	$\delta^{13}\text{C}$ (‰)	Material	Context type	Calibrated date range (95% confidence)	Estimated date range (95% probability)
Worton Rectory Farm Cemetery	UB-3777	SK 2076	1743 ± 21	-20.1±0.2	human bone	articulated skeleton 2016	cal AD 240 – 385	
	UB-3921	SK 2005	1796 ± 21	-19.7±0.2	human bone	articulated skeleton 2005	cal AD 130 – 325	
	UB-3776	SK 1681	2250 ± 21	-20.6±0.2	human bone	articulated skeleton 1681	cal BC 390 – 205	
	UB-3778	SK 2717	2207 ± 21	-20.3±0.2	human bone	articulated skeleton 2717	cal BC 380 – 175	
	UB-3779	SK 2713	2224 ± 21	-20.0±0.2	human bone	articulated skeleton 2713	cal BC 385 – 200	
	UB-3782	SK 376/2	2237 ± 20	-20.0±0.2	human bone	articulated skeleton 376/2	cal BC 390 – 200	
	UB-3919	SK 2710	2168 ± 21	-20.0±0.2	human bone	articulated skeleton 2710	cal BC 355 – 165	
	UB-3920	SK 2718	2234 ± 20	-19.9±0.2	human bone	articulated skeleton 2718	cal BC 385 – 200	
	UB-3922	SK 2069	2268 ± 20	-20.0±0.2	human bone	articulated skeleton 2069	cal BC 400 – 210	
UB-3923	SK 2041	2267 ± 22	-19.9±0.2	human bone	articulated skeleton 2041	Cal BC 385 – 200		
UB-3924	SK 2569	2220 ± 23	-20.0±0.2	human bone	articulated skeleton 2569	Cal BC 385 – 200		
Oxey Mead	OxA-10690	YOM90 3/8	2082 ± 37	-25.9	waterlogged seeds (mixed aerial species)	from basal sediment	cal BC 200 – 10 cal AD	
	OxA-7360	YOM90 3/7	1675 ± 55	-24.5	waterlogged aerial plant macrofossils		cal AD 240 – 540	
Floodplain Section A	OxA-3644	YFP CC/2	2585 ± 75	-27.3	wood, <i>Quercus</i> sp.	post in structure 112	cal BC 900 – 410	
	UB-4060	YFP92 W63 (C112)	2465 ± 18	-26.7±0.2	wood, <i>Quercus</i> sp. sapwood	post in structure 112	cal BC 765 – 410	
	GU-5715	YFP92 115a (W24)	2600 ± 60	-27.8	wood, <i>Quercus</i> sp. roundwood	from layer 115	cal BC 900 – 540	
	GU-5716	YFP92 115b (W34)	2520 ± 50	-26.0	wood, <i>Quercus</i> sp. roundwood	from layer 115	cal BC 800 – 410	
	GU-5717	YFP92 119a (W76)	2520 ± 50	-25.9	wood, <i>Quercus</i> sp. sapwood	post in collapsed wattling 119	cal BC 800 – 410	
	GU-5718	YFP92 119b (W77)	2570 ± 60	-25.1	wood, <i>Quercus</i> sp. roundwood	post in collapsed wattling 119	cal BC 830 – 520	
	UB-4061	YFP92 W126 (C116)	3646 ± 19	-28.1±0.2	wood, Pomoideae	post in structure 116	cal BC 2125 – 1940	
	OxA-10711	YFP92A 37	2098 ± 39	-25.8	waterlogged seeds (mixed aerial species)	from layer 37	cal BC 350 – 1	
	UB-4062	YFP92 W125 (C116)	2567 ± 18	-27.0±0.2	wood, <i>Corylus</i> sp.	post in structure 116	cal BC 800 – 670	
	OxA-10709	YFP92A 32a	2995 ± 45	-26.4	waterlogged seeds, <i>Alnus glutinosa</i>	from layer 32	cal BC 1390 – 1050	
	OxA-10710	YFP92A 32b	3145 ± 45	-26.0	waterlogged seeds (mixed aerial species)	from layer 32	cal BC 1520 – 1310	
	GU-5850	YFP92 109 W99	2970 ± 50	-26.3	wood, <i>Quercus</i> sp. bark and sapwood	from layer 109	cal BC 1380 – 1000	
	GU-5855	YFP92 109 W39	3340 ± 50	-26.2	wood, <i>Quercus</i> sp. (21 heartwood rings), probably centre of a short-lived tree with just the sapwood trimmed off or eroded	from layer 109	cal BC 1750 – 1510	
	UB-4676	W64	2424 ± 16	-27.7±0.2	wood, <i>Quercus</i> sp. roundwood (including sapwood)	post in structure 112	cal BC 760 – 400	
UB-4677	W70	2654 ± 16	-26.6±0.2	wood, <i>Quercus</i> sp. roundwood (including sapwood)	post in structure 112	cal BC 830 – 790		
Floodplain Section B	OxA-10691	YFP92 B/9	2257 ± 37	-25.8	waterlogged seeds (mixed aerial species)	from base of section (layer 9)	cal BC 400 – 200	
	OxA-4816	YFP sample 5	1835 ± 55	-27.6	plant macrofossil	from layer 7	30 – 340 cal AD	
	OxA-7361	YFP sample 6a	1640 ± 50	-25.6	waterlogged plant remains (mixed aerial species)	from layer 6	250 – 540 cal AD	
	OxA-7362	YFP sample 6b	1730 ± 50	-27.0	waterlogged plant remains (mixed aerial species)	from layer 6	130 – 430 cal AD	
Site 2 (alluviation)	OxA-6616	YFP 2835a	2215 ± 45	-27.0	waterlogged seeds (mixed aerial species)	uppermost fill of ditch 2832	cal BC 400 – 160	
	OxA-6618	YFP 2004a	1975 ± 40	-26.5	waterlogged seeds (mixed aerial species)	overbank alluvium	cal BC 50 – 130 cal AD	
Causeways: Site 9	OxA-8703	YFPB98 13263	2175 ± 35	-20.8	animal bone, cattle humerus	bone between stone and gravel causeways	cal BC 370 – 110	

	OxA-8704	YFPB98 13221	2185 ± 40	-21.2	animal bone, cattle radius	bone between stone and gravel causeways	cal BC 390 – 110	
	OxA-10628	YFPB98 18192a	2256 ± 35	-26.0	wood, <i>Salix/Populus</i> sp.	brushwood beneath the stone causeway	cal BC 400 – 200	
	OxA-10629	YFPB98 18136 W168	2198 ± 35	-27.2	wood, <i>Alnus glutinosa</i>	stake forming part of a row beneath the stone causeway	cal BC 390 – 160	
	GU-5852	YFPB98 18006 W2/1	2300 ± 60	-27.1	wood, <i>Quercus</i> sp. (82 rings including 25 sapwood rings)	collapsed handrail lying between stone and gravel causeways	cal BC 490 – 200	
	GU-5853	YFPB98 18031 W26	2330 ± 60	-25.7	wood, <i>Quercus</i> sp (50 rings including 31 sapwood rings and bark)	upright post driven through stone causeway, beneath gravel causeway	cal BC 490 – 200	
	OxA-9377	YFPB98 13266	2275 ± 50	-26.6	waterlogged plant remains	bronze spearhead from beneath stone causeway	cal BC 410 – 200	
	GU-5883	YFPB98 18105 W36	2240 ± 50	-26.7	wood, <i>Quercus</i> sp. sapwood and bark	upright post driven through stone causeway, beneath gravel causeway	cal BC 400 – 170	
Trench 37	OxA-10707	YCE93 37/7	2120 ± 45	-27.4	waterlogged seeds (mixed aerial species)	from lower fill of ditch (context 7)	cal BC 360 – 1	
	OxA-10708	YCE93 37/8	2180 ± 45	-27.1	waterlogged seeds (mixed aerial species)	from basal fill of ditch (context 8)	cal BC 390 – 90	

Draft

Table 13.2: Optically-Stimulated Luminescence measurements

Sample number	Context number	Palaeodose (Gy)	a-value	Total dose rate (Gy/ka)	date (calendar years) (68% confidence)	<i>Estimated date range (95% probability)</i>
957a	4	4.48 ± 0.29	0.105 ± 0.004	2.01 ± 0.14	130 BC – AD 230	
957b	5	4.47 ± 0.30	0.081 ± 0.004	2.24 ± 0.13	160 BC – AD 140	
866a	2/15	3.92 ± 0.22	0.073 ± 0.004	2.29 ± 0.15	AD 140 – 440	
866b	2/5	4.06 ± 0.18	0.086 ± 0.006	2.27 ± 0.16	AD 40 – 360	
866c	2/6	6.27 ± 0.14	0.069 ± 0.002	2.00 ± 0.16	1440 – 860 BC	

Draft